Optical Materials 138 (2023) 113629

Contents lists available at ScienceDirect

Optical Materials

journal homepage: www.elsevier.com/locate/optmat

Research Article

Improving selectivity of thin film solar absorber by cobalt oxide grafted reduced graphene oxide

N. Murugesan [a], S. Suresh [b], S. Murugesan [c], B.K. Balachandar [d], M. Kandasamy [e], N. Pugazhenthiran [f], J. Selvi [g], P. Indira [a], S. Karthick Kumar [a,*]

[a] Department of Physics, Sethu Institute of Technology, Kariapatti, 626 115, Virudhunagar, Tamil Nadu, India
[b] PG & Research Department of Physics, Sri Vidya Mandir Arts & Science College (Autonomous), Katteri, 636 902, Uthangarai, Tamil Nadu, India
[c] Department of Chemistry, School of Chemistry, Madurai Kamaraj University, Madurai, 625 021, Tamil Nadu, India
[d] Department of Physics, Velammal College of Engineering and Technology, Madurai, 625 009, Tamil Nadu, India
[e] Department of Chemistry, K. Ramakrishnan College of Technology, Trichy, 621 112, Tamil Nadu, India
[f] Laboratorio de Fotoquímica y Fotofísica, Departamento de Química, Universidad Técnica Federico Santa María, Av. España 1680, Valparaíso, Chile
[g] The Research Centre of Physics, Fatima College (Autonomous), Madurai, 625 018, Tamil Nadu, India

ARTICLE INFO

Keywords:
Reduced graphene oxide
Cobalt oxide
Nanocomposite
Thin films
Solar selective absorber

ABSTRACT

Reduced graphene oxide (rGO) modified cobalt oxide (Co_3O_4) nanocomposite (NC) thin films were prepared on aluminum substrates through dip-coating technique for solar selective absorber. The prepared rGO-Co_3O_4 NC thin films were characterized by X-ray diffraction, which revealed that the prepared samples have face centered cubic structure. Scanning electron microscopy showed that morphology of prepared thin films is comprised of spherical shaped grains with rough surface. Energy-dispersive X-ray spectra exhibited absence of impurities in the thin films. Raman spectra predicted spinel structure, combined vibrations of tetrahedral site and octahedral oxygen motions in the rGO-Co_3O_4 NC thin films. Optical properties were investigated by UV–Vis–NIR reflectance spectroscopy. The prepared thin films with a concentration of 1.0 wt% of rGO (1%-rGO-Co_3O_4) disclosed a highest solar absorptance ($\alpha = 89.95$) and low thermal emittance ($\varepsilon = 4.6$) with a highest solar selectivity (ξ) of 19.55. These values indicated that the rGO-Co_3O_4 NC thin film samples can be ideal candidates as solar selective absorbers for solar thermal energy gadgets.

1. Introduction

Solar energy has manifested as highly ideal, copious and reliable energy resource when compared to other renewable energy resources [1,2]. Among diverse technologies that reliant on solar energy, solar thermal technology is regarded as eco-friendly that directly transforms solar energy into thermal energy and consequently, it finds application in the fields of solar water heating, concentrating solar collectors, seawater desalination, solar thermoelectric and solar assisted cooling of buildings [3–6]. A key device component, which is necessitated in all these applications for harvesting thermal form of solar energy is solar selective absorber with significant solar absorptance ($\alpha > 90\%$) in visible and near-infrared regions (0.4 μm–2.0 μm) and low thermal emittance ($\varepsilon < 10\%$) in mid-infrared wavelengths (2.5 μm–25 μm) of the solar spectrum (Planck's spectrum) [7,8]. Materials with appreciable photothermal conversion potential can be developed with an aid of their anticipated properties of high thermal conductivity, notable thermal stability, long-term humidity tolerance, corrosion resistance, small refraction index and low expansion coefficient [9]. Nevertheless, previous studies have been conclusively demonstrated the possibility of not attaining considerably high photothermal conversion efficiencies by a single-component solar selective absorber [10–13]. Conversely, high photothermal conversion efficiencies can be attained using bi-component functional materials by means of their improved properties over single-component materials [14]. It has been proved that the low-cost metal substrate (Aluminum (Al)) employed for coating solar selective absorber discloses beneficial properties of low thermal emittance, appreciable thermal conductivity and resistance to corrosion [15].

Recently, research interest on cobalt oxide (Co_3O_4) has increased because of its high surface area, affordability, eco-friendly, facile fabrication, and outstanding chemical, physical and corrosion stability.

* Corresponding author.
E-mail address: physicsmsckarthick@gmail.com (S. Karthick Kumar).

https://doi.org/10.1016/j.optmat.2023.113629
Received 1 December 2022; Received in revised form 12 February 2023; Accepted 22 February 2023
Available online 17 March 2023

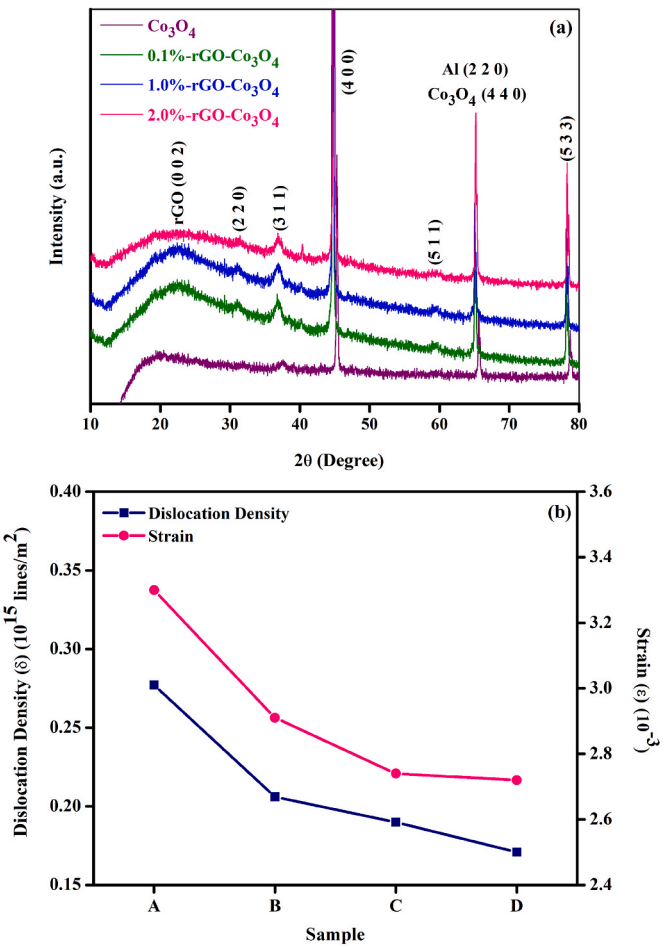

Fig. 1. (a) XRD spectra of Co_3O_4 and rGO-Co_3O_4 NC thin films and (b) Dislocation density and strain values of (A) Co_3O_4, (B) 0.1%-rGO-Co_3O_4, (C) 1.0%-rGO-Co_3O_4 and (D) 2.0%-rGO-Co_3O_4 NC thin films.

It is a p-type semiconductor with band gap energy ranges between 1 and 3 eV [16–18]. Owing to outstanding optical, electrical and magnetic properties, it has been found diverse application potentials in gas sensors [19], supercapacitors [20], lithium-ion batteries [21], low temperature CO oxidation [22], high temperature solar selective absorbers [23] and energy storage [24]. Among several solar selective absorber coatings, Co_3O_4 has been investigated as an inherent solar selective absorber in view of its advantageous properties of low thermal emittance and high solar absorptance [17,18,23]. Meanwhile, in recent years, researchers have switched over their attention significantly to graphene because of its unique thermal, physical and chemical properties. Graphene has attained considerable attraction because of its interesting large theoretical surface area (2630 m^2g^{-1}), substantial intrinsic mobility, high Young's modulus (1.0 T Pa), appreciable thermal conductivity (5000 $Wm^{-1}K^{-1}$) and noticeable transmittance (97.7%). In addition, it has shown exceptional electrical conductivity, mechanical flexibility, optical transparency and low thermal expansion coefficient [25–29]. As a consequence, it has found proficient application potentials in catalysis, sensors, energy conversion and energy storage devices.

Two imperative derivatives of graphene are graphene oxide (GO) and reduced graphene oxide (rGO) that disclose different chemical and structural characteristics, due to variations in their chemical composition. The most noticeable differences are found in their thermal stability, electrical conductivity, mechanical strength, hydrophilic behavior, and dispersibility. The stability of GO with respect to temperature can be improved by reducing GO partially, which produces rGO and moreover that induces key changes in mechanical, structural, solubility and reactive properties [30]. Consequently, the rGO exhibits substantial application potential in sensors [31,32], storage of energy and its conversion, electronic devices, supercapacitors, biomedicine, catalysts and water purification [33]. Noticeably, the rGO has marked absorption property in visible and near infrared regions of the solar spectrum [34,35] and as a result, it can be integrated as an ideal component for solar selective absorber. Recently, the rGO has demonstrated as a most promising tandem material for improving efficiency of solar selective absorber in combination with NiO [36]. Meanwhile, it contains functional groups that facilitate its dispersion in a variety of solvents without aggregation [37,38]. Optimizing optical properties of inorganic semiconductor metal oxide in combination with rGO as a hybrid system is feasible for the development of rGO-based solar selective absorber. Since the rGO facilitates considerable solubility in aqueous and polar solvents, the dependance of sol-gel technique is viable to prepare rGO-based thin films, which could display high transmittance and strongly resist abrasion that is ideal for applications during harsh conditions [39].

Formation of economically and optically efficient solar selective absorber is an indispensable prerequisite for realizing low-cost solar flat plate thermal collectors because the present solar selective absorbers preparation methods need costly equipment and also they are not eco-friendly. In this work, we demonstrate the synthesis of low-cost solar-selective absorber thin films comprised of Co_3O_4 grafted rGO on Al substrates through a simple dip-coating technique. The goal of the present work is to realize an efficient solar selective absorber nanocomposite thin film by combination of Co_3O_4 with optically efficient rGO.

2. Experimental

2.1. Chemicals

Graphite flakes were procured from Alfa Aesar. Sulfuric acid (H_2SO_4), potassium permanganate ($KMnO_4$), hydrogen peroxide (H_2O_2) and sodium nitrate ($NaNO_3$) were supplied by Rankem. Cobalt acetate [$Co(CH_3COO)_2$], diethanolamine (DEA) [$NH(CH_2CH_2OH)_2$] and polyethylene glycol (PEG) [$HO(CH_2CH_2O)nH$, MW = 4000] were procured from Merck. Ethanol [CH_3CH_2OH] and double distilled water were employed for experiments.

2.2. Preparation of Co_3O_4 precursor sol

The Co_3O_4 precursor sol was prepared by dissolving 0.6 M cobalt acetate in absolute ethanol and subjected to magnetic stirring for 4 h. By heating the above solution at 50 °C for 20 min, ethanol was evaporated and reduced to half of its volume to get an adhesive solution. Subsequently, DEA was added as a chelating agent and stirred for 30 min, followed by PEG was included to the Co_3O_4 precursor sol as structure directing agent and the stirring was continued.

2.3. Preparation of rGO-Co_3O_4 nanocomposite thin films

Modified Hummer's protocol was employed to prepared graphene oxide (GO) from natural graphite [40]. Afterwards, diverse quantities (0.1, 0.2, 0.5, 1.0, 1.5 and 2.0 wt%) of GO were mixed separately to the Co_3O_4 precursor sol. Eventually, the composite sols were stirred for 24 h and aged for 5 days to form sols containing GO-Co_3O_4 nanocomposites. The precleaned Al substrates were subjected to dip coating by immersing them in the GO-Co_3O_4 NC sols using dip coating equipment. The dipping and withdrawal rates of the Al substrates were 2 mm/s and the evaporation time of the coating on the Al substrate was 10 s. Finally, the coated thin films were dried at 100 °C for 4 h and calcined at 250 °C in a muffle furnace for 3 h to get rGO-Co_3O_4 NC thin films.

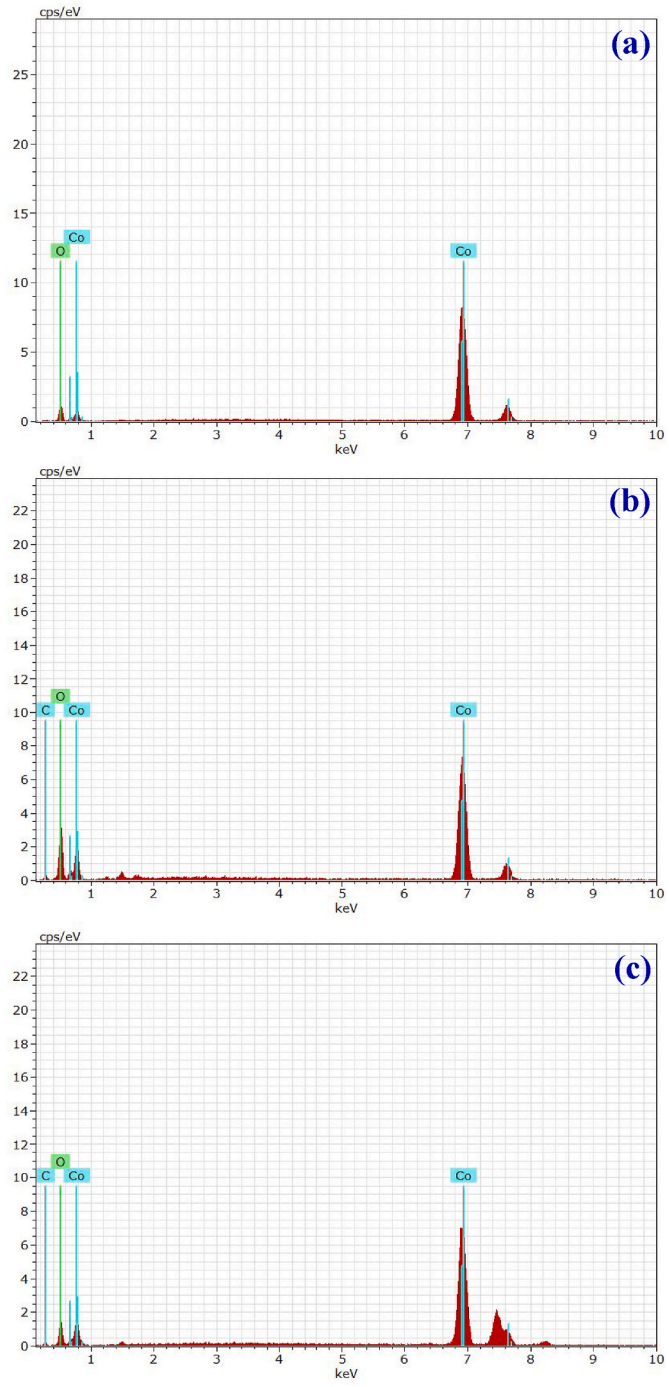

Fig. 2. EDX spectra of (a) Co_3O_4, (b) 1.0%-rGO-Co_3O_4 and (c) 2.0%-rGO-Co_3O_4 NC thin films.

2.4. Characterization

XRD patterns of rGO-Co_3O_4 NC thin films were recorded in Bruker AXS D8 advance X-ray diffractometer with Cu Kα radiation (λ = 1.5418 Å). SEM images and EDX spectra were taken using JEOL6390 scanning electron microscopy and EDX accessory, respectively. Raman spectra were obtained by 632.8 nm line of the He-Ne laser as excitation source. Normal reflectance of thin films was measured between 400 and 2200 nm using UV–vis–NIR spectrophotometer (Cary 5E) equipped with DRS accessory. Solar absorptances of thin films were calculated by the following formula [41]:

Table 1
Elemental composition of Co_3O_4 and rGO-Co_3O_4 NC thin films with different weight percentages.

Thin Film Sample	Elements Present	Series	Weight%	Atomic%
Co_3O_4	Co	K-Series	85.59	61.73
	O		14.41	38.27
1%-rGO-Co_3O_4 NC	Co	K-Series	60.14	28.09
	O		34.02	58.52
	C		5.84	13.39
2%-rGO-Co_3O_4 NC	Co	K-Series	73.85	41.49
	O		19.77	40.92
	C		6.38	17.59

$$Absorp\tan ce(\alpha) = \frac{\int_{0.3\mu m}^{2.0\mu m} I_{sol}(\lambda)(1 - R(\lambda))d\lambda}{\int_{0.3\mu m}^{2.0\mu m} I_{sol}(\lambda)d\lambda} \quad (1)$$

where, $I_{sol}(\lambda)$ is normal spectral irradiance of solar radiation at wavelength 'λ'.

Thermal emittance was recorded in an emissometer (AE1/RD1). The selectivity (ξ) of thin films is ratio between solar absorptance (α) to thermal emittance (ε).

$$\xi = \frac{\alpha}{\varepsilon} \quad (2)$$

3. Results and discussion

3.1. XRD analysis

XRD spectra of Co_3O_4, 0.1%-rGO-Co_3O_4, 1.0%-rGO-Co_3O_4 and 2.0%-rGO-Co_3O_4 NC thin films are illustrated in Fig. 1(a). The XRD pattern of pure Co_3O_4 thin film exhibits diffraction peaks correspond to stable Co_3O_4 phase at 2θ values of 31.69, 37.63, 45.29, 60.34, 65.67, and 78.73°, which are allocated to (2 2 0), (3 1 1), (4 0 0), (5 1 1), (4 4 0) and (5 3 3) diffraction planes of face centered cubic structured Co_3O_4 (JCPDS Card No. 42-1467) [18,42]. The diffraction peak appeared at 65.43° corresponding to the (2 2 0) diffraction plane is attributed to the Al substrate [43]. XRD spectra of rGO-Co_3O_4 NC thin films with diverse weight percentages (0.1, 1.0, and 2.0 wt%) of GO disclose diffraction peaks at 2θ values of 31.23, 36.90, 44.71, 59.68, 65.07, and 78.20°. In addition to the diffraction peaks of Co_3O_4, a broad diffraction peak belongs to rGO is appeared at 22.69° (0 0 2) in XRD patterns of the rGO-Co_3O_4 NC thin films. It is detected visibly that each diffraction peak has marginally shifted to lower diffraction angles with respect to diffraction peak positions of pure Co_3O_4 thin film. This slight shift in the diffraction peaks is due to the presence of rGO in the rGO-Co_3O_4 NC thin films. Similarly, diffraction peaks of rGO-Co_3O_4 NC thin films have shown different intensity values because of the influence of different weight percentages of rGO in the rGO-Co_3O_4 NC thin films and film thickness.

The crystallite size (D) of pure Co_3O_4 and 0.1%-rGO-Co_3O_4, 1.0%-rGO-Co_3O_4 and 2.0%-rGO-Co_3O_4 NC thin films was calculated by Scherrer's formula [44] and values were found to be 60.10, 69.55, 72.46, and 76.41 nm, respectively. It is ascertained that crystallite sizes of 0.1%-rGO-Co_3O_4, 1.0%-rGO-Co_3O_4 and 2.0%-rGO-Co_3O_4 NC thin films are considerably high when compared to pure Co_3O_4 thin film owing to the existence of rGO in the rGO-Co_3O_4 NC thin films. The crystallite size values were used to calculate dislocation density (δ) and strain (ε) of the thin films and the obtained values are shown in Fig. 1(b). Basically, number of defects in a crystal is described by dislocation density and crystallinity is explained with the help of strain. From Fig. 1

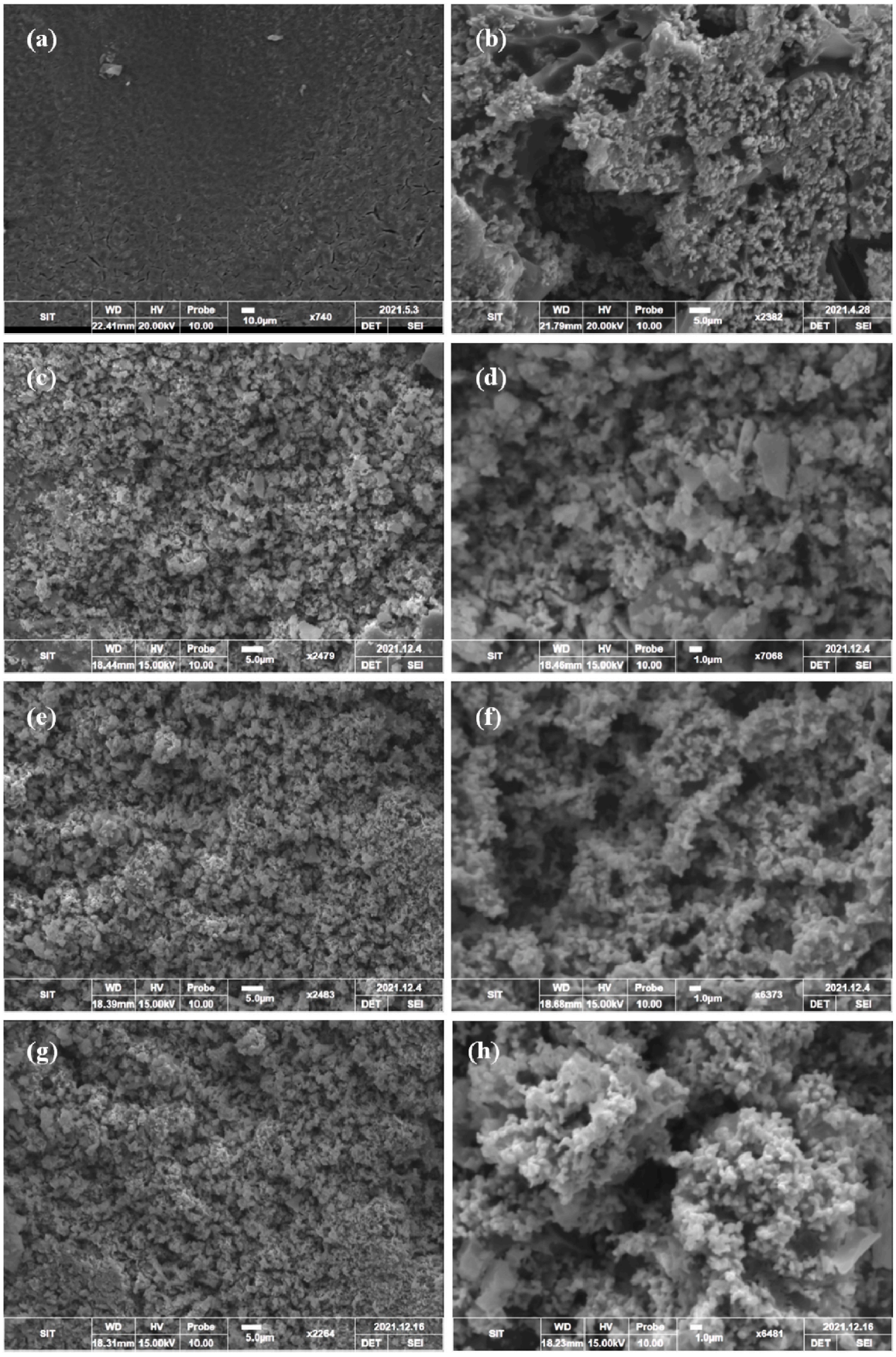

Fig. 3. SEM images of Co_3O_4 (a & b) thin film and 0.1%-rGO-Co_3O_4 (c & d), 1.0%-rGO-Co_3O_4 (e & f) and 2.0%-rGO-Co_3O_4 (g & h) NC thin films.

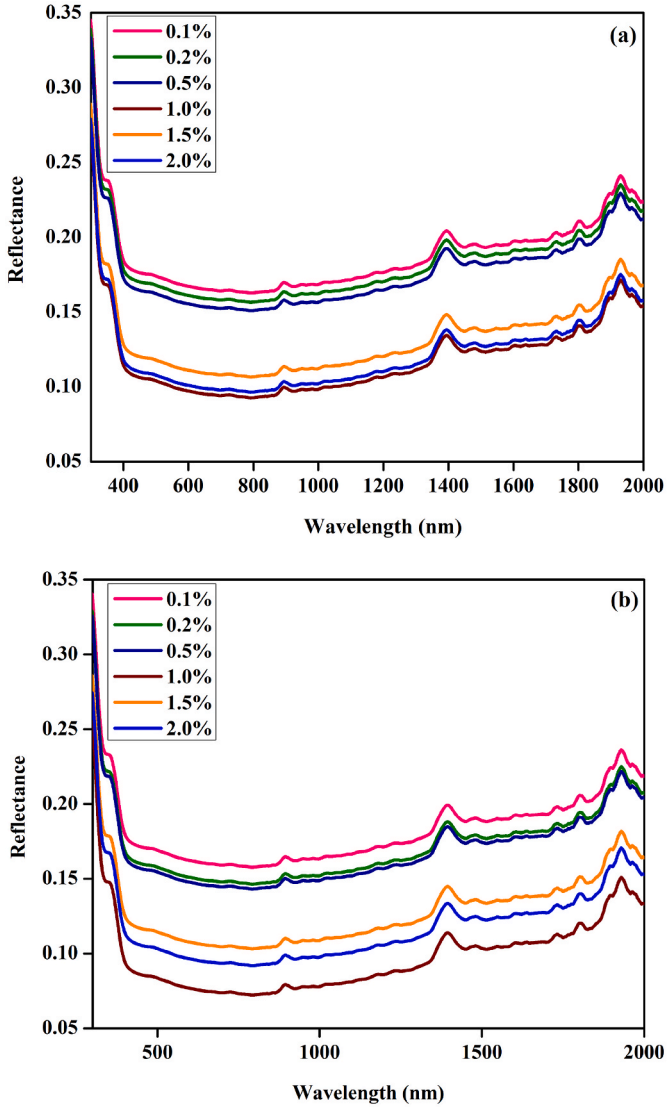

Fig. 4. UV–Vis reflectance spectra of rGO-Co_3O_4 NC thin films prepared using (a) 10 dipping and (b) 20 dipping.

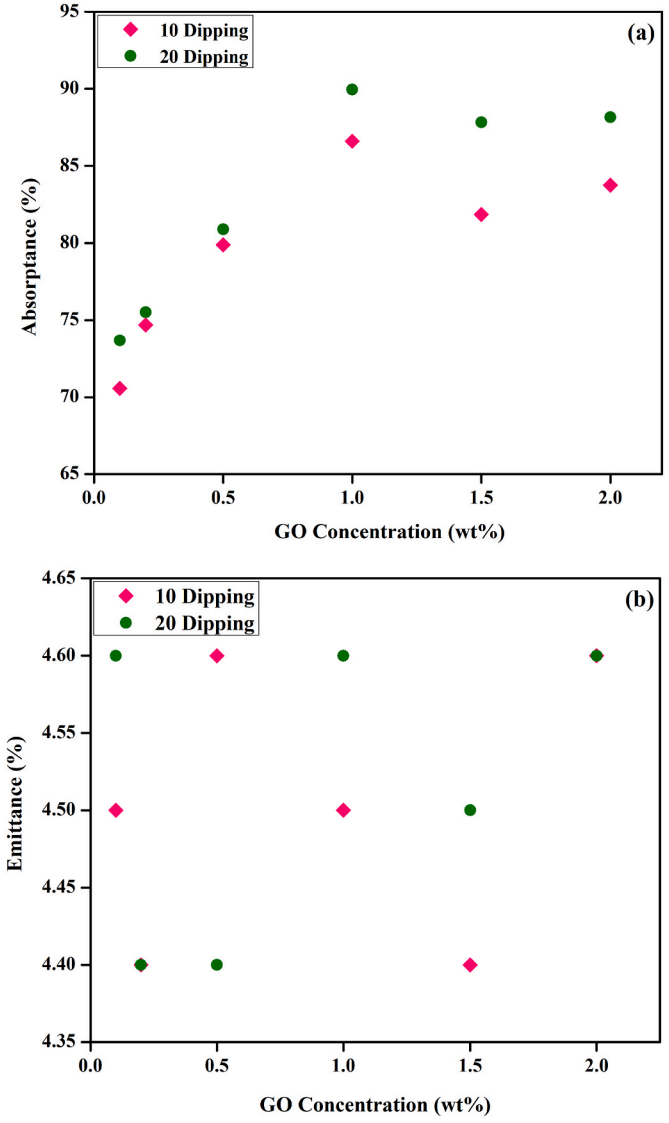

Fig. 5. Absorptance (a) and emittance (b) values of rGO-Co_3O_4 NC thin films.

(b), it is noticed that pure Co_3O_4 thin film has exhibited highest dislocation density and strain values whereas, the values have decreased for rGO-Co_3O_4 NC thin films with respect to increasing the weight percentage of rGO in the rGO-Co_3O_4 NC thin films. This lower value of dislocation density shows degree of crystallization of coated films and minimum strain value strongly indicates improved crystallinity of rGO-Co_3O_4 NC thin films.

3.2. EDX study

EDX characterization were performed to examine presence of elements in Co_3O_4, 1.0%-rGO-Co_3O_4 and 2.0%-rGO-Co_3O_4 NC thin films and the obtained EDX spectra and percentage elemental composition are shown in Fig. 2 and Table 1, respectively. The purity of Co_3O_4 thin film is ascertained by its corresponding EDX spectrum, which discloses peaks with respect to the elements of Co and O (Fig. 2(a)). The atomic weight percentage of Co and O in the Co_3O_4 thin film is found to be 61.73 and 38.27%, respectively (Table 1). Conversely, EDX spectra of both 1.0%-rGO-Co_3O_4 and 2.0%-rGO-Co_3O_4 NC thin films displayed peaks belong to the elements of Co, O, and C (Fig. 2(b) and (c)). The presence of carbon in the 1.0%-rGO-Co_3O_4 and 2.0%-rGO-Co_3O_4 NC thin films firmly confirmed the existence of rGO. The atomic weight percentage of the Co, O, and C are 28.09, 58.52, and 13.39%, respectively for the 1.0%-rGO-Co_3O_4 thin film and 41.49, 40.92, and 17.59%, respectively for the 2.0%-rGO-Co_3O_4 NC thin film (Table 1). The purity of 1.0%-rGO-Co_3O_4 and 2.0%-rGO-Co_3O_4 NC thin films is confirmed by absence of peaks related to foreign elements.

Table 2
Selectivity (ξ) of rGO-Co_3O_4 NC thin films.

Wt% of GO	Selectivity (ξ)	
	10 Dipping	20 Dipping
0.1%	15.68	16.01
0.2%	16.97	17.16
0.5%	17.36	18.38
1.0%	19.24	19.55
1.5%	18.60	19.52
2.0%	18.20	19.16

3.3. SEM examination

SEM was used to determine the morphology of pure Co_3O_4, 0.1%-rGO-Co_3O_4, 1.0%-rGO-Co_3O_4 and 2.0%-rGO-Co_3O_4 NC thin films and

Table 3
Comparison of optical properties of rGO-Co_3O_4 NC thin film with previous reports.

Solar Selective Absorber	Substrate	Coating Method	Absorptance, α (%)	Emittance, ε (%)	Selectivity, (ξ)	Reference
Co–Al_2O_3 cermet	Stainless steel	Spray pyrolysis	82.70	6.0	13.69	[45]
rGO-NiO NC	Al	Dip-coating	88.03	4.5	19.56	[36]
ZrB_2/Al_2O_3	Stainless steel	Magnetron sputtering	92.00	11.0	8.36	[46]
GO-$Cu_xCo_yO_z$	Al	Dip-coating	86.14	2.97	29.01	[39]
TiAlN/AlON tandem	Cu	Magnetron sputtering	94.20	5.0	18.80	[47]
HfB_2/Al_2O_3 tandem	Stainless steel	Magnetron sputtering	92.00	10.9	8.44	[48]
$Al/Si_3N_4/(Ti/Si_3N_4)^2$	Silicon	Magnetron sputtering and PECVD	94.00	7.0	13.40	[49]
Bilayer WO_x/SiO_2	Al	Magnetron sputtering	92.30	5.4	17.09	[7]
Ag–CuO NC	Stainless steel	Dip-coating	92.00	5.0	18.40	[50]
$Cu/TiN_xO_y/Si_3N_4/SiO_2$	Glass	Magnetron sputtering	97.50	3.7	26.20	[51]
rGO-Co_3O_4 NC	Al	Dip-coating	89.95	4.4	19.55	Present Work

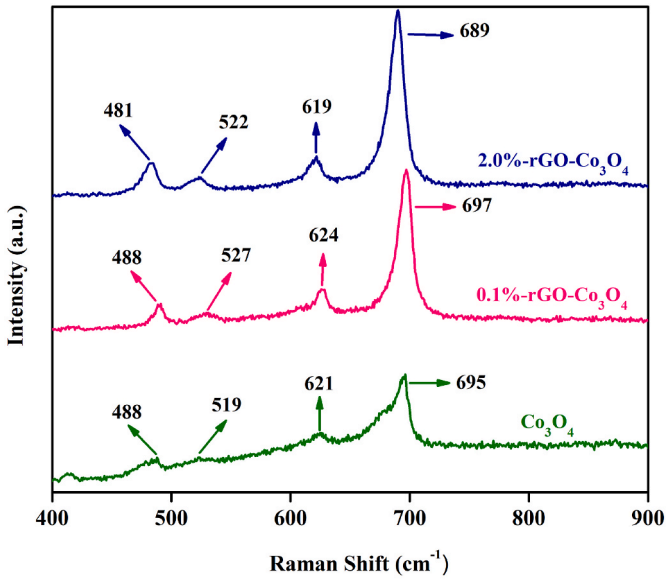

Fig. 6. Raman spectra of pure Co_3O_4 thin film, 0.1%-rGO-Co_3O_4 and 2.0%-rGO-Co_3O_4 NC thin films.

the recorded low and high magnification SEM images are displayed in Fig. 3(a–h). The low magnification SEM image of pure Co_3O_4 thin film (Fig. 3(a)) shows that the Co_3O_4 is uniformly deposited on Al substrate. Even though low magnification SEM images of all the samples illustrate presence of fine coating Fig. (3(a, c, e and g)), the films have roughness on their surface. The high magnification SEM images Fig. (3(b, d, f and h)) exhibit spherical shaped particles dispersed on the Al substrate. The high magnification SEM image of 2.0%-rGO-Co_3O_4 NC thin film possesses spherical nanoparticles on thin films with an average size of ~175 nm (Fig. 3(h)). The high magnification SEM images of the rGO-Co_3O_4 NC thin films reveal that many spherical grain like Co_3O_4 particles are disseminated randomly on the rGO sheets Fig. (3(d, f and h)). The polymer (PEG) in the precursor sol can help the rGO to adsorb the Co_3O_4 grains with an aid of surface functional groups. As a consequence of various wt% of rGO and PEG, the different grain sized Co_3O_4 particles are outspread on the rGO sheet in a productive manner.

3.4. UV–Vis–NIR spectroscopy investigation

UV–Vis–NIR reflection spectra of rGO-Co_3O_4 NC thin films prepared using diverse weight percentages (0.1%–2.0%) of rGO are shown in Fig. 4. The variations in reflectance of the rGO-Co_3O_4 NC thin films in UV–Vis–NIR region are easily observed from Fig. 4. The thin films displayed low reflectance (<5%) in visible region and relatively high reflectance (>35%) in infrared region. It is presumed that the exterior of Al substrate helps to reflect infrared radiation that infiltrates through the coated thin films because of its inherent property of high reflectivity. The absorptance and reflectance of rGO-Co_3O_4 NC thin films are influenced by parameters, such as film thicknesses, exterior roughness and rGO content. The thickness of rGO-Co_3O_4 NC thin films was varied by adopting the thin films to different numbers of dipping (10 and 20) using dip-coating technique. The increment in the thin film thickness could diminish the reflectance, which helps to get a better outcome so that the rGO-Co_3O_4 NC thin films prepared using 10 dipping have displayed slightly high reflectance and low absorptance in the visible spectral region when compared to the thin films fabricated using 20 dipping. From the UV–Vis–NIR spectra (Fig. 4(a)), the 1.0%-rGO-Co_3O_4 thin film has showed low reflectance among the different rGO-Co_3O_4 NC thin films prepared using 10 dipping. This can be ascribed that the 1.0%-rGO-Co_3O_4 thin film prepared using 1.0 wt% of rGO would be appropriate to facilitate a greater number of active sites for high absorption. The aforementioned rGO-Co_3O_4 NC thin films prepared using 10 dipping have disclosed high reflectance when compared to the rGO-Co_3O_4 NC thin films produced by 20 dipping as a consequence of film thickness (Fig. 4(a and b)).

The absorptance values of rGO-Co_3O_4 NC thin films were calculated from their respective reflectance spectra and their corresponding emittance values were measured using emissometer, which are shown in Fig. 5(a and b). The GO content is considered as a chief factor that influences optical properties of the rGO-Co_3O_4 NC thin films. The SEM images (Fig. 3(d, f and h)) show that the rGO act as host material for spherical shaped Co_3O_4 grains and as a consequence, the absorbance of the resultant rGO-Co_3O_4 NC thin films has increased. In the rGO-Co_3O_4 NC thin films, the exterior shows pores in the coated surface, which also help to increase the absorptance of the thin films since the holes could help to happen multiple reflection within the thin films. The rGO-Co_3O_4 NC thin films prepared using different dipping and diverse content of GO had shown different absorptance (α = 70.56 to 89.95) and emittance (ε = 4.4 to 4.6) values. From the calculated absorptance values, when the concentration of GO increases, the absorptance value of rGO-Co_3O_4 NC thin films increases. This suggests that optical properties of rGO-Co_3O_4 NC thin films is mainly influenced by the GO content. The calculated solar spectral selectivity of the rGO-Co_3O_4 NC thin films has increased from 15.68 to 19.55 (Table 2), which revealed that the prepared rGO-Co_3O_4 NC thin films have good solar selectivity. The comparison of optical properties of the rGO-Co_3O_4 NC thin film with previous reports are given in Table 3.

3.5. Raman spectroscopy analysis

Fig. 6 shows Raman spectra of pure Co_3O_4 thin film and 0.1%-rGO-Co_3O_4 and 2.0%-rGO-Co_3O_4 NC thin films. The Raman peaks were observed for Co_3O_4 thin film at 485, 519, 621, and 695 cm^{-1}. The spinel structure was predicted by these Raman active peaks for Co_3O_4. The

octahedral sites characteristics were assigned for the Raman mode at 695 cm^{-1} (A_{1g}), continuously the peaks at 485 cm^{-1} (E_g) and 621 cm^{-1} (F_{2g}) are possibly associated with combined vibrations of tetrahedral site and octahedral oxygen motions. To take into consideration and significance of the rGO content on the Raman spectra, the measurement of Raman spectra were recorded for the thin film samples before and after the incorporation of rGO. The Raman peaks for low and high contents of rGO were obtained for 488, 527, 624, and 697 cm^{-1} and 481, 522, 619, and 689 cm^{-1}, respectively. These peak positions are slightly changed from the peaks observed for the pure Co_3O_4 thin film. This alteration could be caused by the composition of rGO. On the other hand, the intensity of the nanocomposite samples has higher value than the pure Co_3O_4, subsequently there is also intensity difference between the thin films having low and high rGO content. The Raman spectrum obtained for the samples show broad bands for Co_3O_4 thin film and narrow bands for composite thin films, especially the 2.0%-rGO-Co_3O_4 NC thin film has relatively intense narrow bands when compared to other thin film samples. These results are matched with the crystalline size calculated from XRD data by Scherrer's formula, which exhibits that the 2.0%-rGO-Co_3O_4 NC thin film has larger crystallite size (76.41 nm) [20,52,53].

4. Conclusion

Reduced Graphene Oxide (rGO) modified cobalt oxide (Co_3O_4) NC thin films on aluminum substrates were prepared through dip-coating technique for solar selective absorbers. XRD patterns of rGO-Co_3O_4 NC thin films exhibited diffraction peaks corresponding to face centered cubic structured Co_3O_4 and rGO. SEM images showed morphology of the prepared samples have spherical shaped grains with rough surface. EDX spectra disclosed the samples with absence of impurities. The presence of rGO in the rGO-Co_3O_4 NC thin films were further concretely confirmed by Raman analysis. The optical properties investigated by UV–Vis–NIR reflectance spectroscopy revealed that the rGO-Co_3O_4 NC thin film with rGO content of 1.0 wt% has high absorptance of 89.95, thermal emittance of 4.6 and consequently high solar selectivity of 19.55.

CRediT authorship contribution statement

N. Murugesan: Conceptualization, Methodology, Data curation, Validation, Formal analysis, Investigation, Writing - original draft. **S. Suresh:** Data curation, Formal analysis, Software, Writing – review & editing, Visualization, Validation. **S. Murugesan:** Conceptualization, Supervision, Validation, Visualization, Writing - review & editing. **B.K. Balachandar:** Data curation, Formal analysis, Software, Visualization, Validation. **M. Kandasamy:** Data curation, Formal analysis, Software, Validation. **N. Pugazhenthiran:** Formal analysis, Software, Writing – review & editing, Validation. **J. Selvi:** Formal analysis, Software, Visualization, Validation. **P. Indira:** Formal analysis, Software, Visualization, Validation. **S. Karthick Kumar:** Conceptualization, Supervision, Resources, Project administration, Writing – review & editing, Validation.

Declaration of competing interest

The authors declare that they have no known competing financial interests or personal relationships that could have appeared to influence the work reported in this paper.

Data availability

Data will be made available on request.

Acknowledgement

The authors (N. Murugesan and S. Karthick Kumar) express their gratefulness to SERB, Government of India, New Delhi, India for financially supporting this work through Early Career Research Award Scheme (ECR/2016/002017) and FIST Programme, R & D (Infrastructure) Division, New Delhi, India for instrumentation support (SR/FST/College-326.2016(C)). S. Suresh express his gratitude to the DST, Government of India, New Delhi for generously providing Instrumentation Facility through FIST Programme (Grant No. SR/FST/College-2017/140 (C), dt. 14.08.2018).

References

[1] G. Li, S. Shittu, T.M.O. Diallo, M. Yu, X. Zhao, J. Ji, A review of solar photovoltaic-thermoelectric hybrid system for electricity generation, Energy 158 (2018) 41–58, https://doi.org/10.1016/j.energy.2018.06.021.
[2] S.R. Atchuta, S. Sakthivel, H.C. Barshilia, Nickel doped cobaltite spinel as a solar selective absorber coating for efficient photothermal conversion with a low thermal radiative loss at high operating temperatures, Sol. Energy Mater. Sol. Cells 200 (2019), 109917, https://doi.org/10.1016/j.solmat.2019.109917.
[3] K. Zhang, L. Hao, M. Du, J. Mi, J.-N. Wang, J.-p. Meng, A review on thermal stability and high temperature induced ageing mechanisms of solar absorber coatings, Renew. Sustain. Energy Rev. 67 (2017) 1282–1299, https://doi.org/10.1016/j.rser.2016.09.083.
[4] A. Dan, H.C. Barshilia, K. Chattopadhyay, B. Basu, Solar energy absorption mediated by surface plasma polaritons in spectrally selective dielectric-metal-dielectric coatings: a critical review, Renew. Sustain. Energy Rev. 79 (2017) 1050–1077, https://doi.org/10.1016/j.rser.2017.05.062.
[5] D. Jiang, Z. Fan, M. Dong, Y. Shang, X. Liu, G. Chen, S. Li, Titanium nitride selective absorber enhanced solar thermoelectric generator (SA-STEG), Appl. Therm. Eng. 141 (2018) 828–834, https://doi.org/10.1016/j.applthermaleng.2018.06.032.
[6] N.H. Thomas, Z. Chen, S. Fan, A.J. Minnich, Semiconductor-based multilayer selective solar absorber for unconcentrated solar thermal energy conversion, Sci. Rep. 7 (2017) 5362, https://doi.org/10.1038/s41598-017-05235-x.
[7] H. Wen, W. Wang, W. Wang, J. Su, T. Lei, C. Wang, Enhanced spectral absorption of bilayer WO_x/SiO_2 solar selective absorber coatings via low vacuum pre-annealing, Sol. Energy Mater. Sol. Cells 202 (2019), 110152, https://doi.org/10.1016/j.solmat.2019.110152.
[8] S.K. Kumar, S. Murugesan, S. Suresh, Preparation and characterization of CuO nanostructures on copper substrate as selective solar absorbers, Mater. Chem. Phys. 143 (2014) 1209–1214, https://doi.org/10.1016/j.matchemphys.2013.11.023.
[9] M. Bello, S. Shanmugan, Achievements in mid and high-temperature selective absorber coatings by physical vapor deposition (PVD) for solar thermal application-A review, J. Alloys Compd. 839 (2020), 155510, https://doi.org/10.1016/j.jallcom.2020.155510.
[10] P. Oelhafen, A. Schuler, Nanostructured materials for solar energy conversion, Sol. Energy 79 (2005) 110–121, https://doi.org/10.1016/j.solener.2004.11.004.
[11] H.C. Barshilia, N. Selvakumar, K.S. Rajam, D.V.S. Rao, K. Muraleedharan, Deposition and characterization of TiAlN/TiAlON/Si_3N_4 tandem absorbers prepared using reactive direct current magnetron sputtering, Thin Solid Films 516 (2008) 6071–6078, https://doi.org/10.1016/j.tsf.2007.10.113.
[12] A. Amri, Z.T. Jiang, T. Pryor, C.-Y. Yin, S. Djordjevic, Developments in the synthesis of flat plate solar selective absorber materials via sol–gel methods: a review, Renew. Sustain. Energy Rev. 36 (2014) 316–328, https://doi.org/10.1016/j.rser.2014.04.062.
[13] S.K. Kumar, S. Murugesan, S. Suresh, Anodization assisted preparation of diverse nanostructured copper oxide films for solar selective absorber, Opt. Mater. 135 (2023), 113304, https://doi.org/10.1016/j.optmat.2022.113304.
[14] R. Yang, D. Tang, T. Tao, Y. Ren, X. Zhang, M. Xu, C. Wang, One-step green synthesis of hierarchical hydrangea shaped Cu_2O–CuO composite, Mater. Lett. 113 (2013) 156–158, https://doi.org/10.1016/j.matlet.2013.09.082.
[15] J.A. Wahab, M.N. Derman, Characterization of porous anodic aluminium oxide film on aluminium templates formed in anodizing process, Adv. Mater. Res. 173 (2011) 55–60. https://doi.org/10.4028/www.scientific.net/AMR.173.55.
[16] S.G. Kandalkar, J.L. Gunjakar, C.D. Lokhande, Preparation of cobalt oxide thin films and its use in supercapacitor application, Appl. Surf. Sci. 254 (2008) 5540–5544, https://doi.org/10.1016/j.apsusc.2008.02.163.
[17] H.E. Aakib, N. Rochdi, J.F. Pierson, A. Outzourhit, Reactively sputtered cobalt oxide coatings for solar selective absorber applications, Mater. Today Proc. 39 (2021) 1157–1162, https://doi.org/10.1016/j.matpr.2020.07.562.
[18] D.A. Vázquez-Vargas, P. Amézaga-Madrid, L.E. Jáuregui-Martínez, O. Esquivel-Pereyra, W. Antúnez-Flores, P. Pizá-Ruiz, M. Miki-Yoshida, Synthesis and microstructural characterization of cupric oxide and cobalt oxide nanostructures for their application as selective solar coatings, Thin Solid Films 706 (2020), 138046, https://doi.org/10.1016/j.tsf.2020.138046.
[19] S. Vetter, S. Haffer, T. Wagner, M. Tiemann, Nanostructured Co_3O_4 as a CO gas sensor: temperature-dependent behavior, Sensor. Actuator. B Chem. 206 (2015) 133–138, https://doi.org/10.1016/j.snb.2014.09.025.
[20] Y. Tao, Y. Wu, H. Chen, W. Chen, J. Wang, Y. Tong, G. Pei, Z. Shen, C. Guan, Synthesis of amorphous hydroxyl-rich Co_3O_4 for flexible high-rate supercapacitor, Chem. Eng. J. 396 (2020), 125364, https://doi.org/10.1016/j.cej.2020.125364.
[21] R.W. Kennedy, K.C. Marr, O.A. Ezekoye, Gas release rates and properties from Lithium Cobalt Oxide lithium ion battery arrays, J. Power Sources 487 (2021), 229388, https://doi.org/10.1016/j.jpowsour.2020.229388.

[22] J. Bae, D. Shin, H. Jeong, B.-S. Kim, J.W. Han, H. Lee, Highly water-resistant La-doped Co_3O_4 catalyst for CO oxidation, ACS Catal. 9 (2019) 10093–10100, https://doi.org/10.1021/acscatal.9b02920.
[23] S.A. Makhlouf, Z.H. Bakr, K.I. Aly, M.S. Moustafa, Structural, electrical and optical properties of Co_3O_4 nanoparticles, Superlattice. Microst. 64 (2013) 107–117, https://doi.org/10.1016/j.spmi.2013.09.023.
[24] S. Xiong, M. Lin, L. Wang, S. Liu, S. Weng, S. Jiang, Y. Xu, Y. Jiao, J. Chen, Defects-type three-dimensional Co_3O_4 nanomaterials for energy conversion and low temperature energy storage, Appl. Surf. Sci. 546 (2021), 149064, https://doi.org/10.1016/j.apsusc.2021.149064.
[25] Q. Zheng, B. Zhang, X. Lin, X. Shen, N. Yousefi, Z.-D. Huang, Z. Li, J.-K. Kim, Highly transparent and conducting ultralarge graphene oxide/single-walled carbon nanotube hybrid films produced by Langmuir–Blodgett assembly, J. Mater. Chem. 22 (2012) 25072–25082, https://doi.org/10.1039/c2jm34870e.
[26] J. Yan, Z. Fan, W. Sun, G. Ning, T. Wei, Q. Zhang, R. Zhang, L. Zhi, F. Wei, Advanced asymmetric supercapacitors based on $Ni(OH)_2$/graphene and porous graphene electrodes with high energy density, Adv. Funct. Mater. 22 (2012) 2632–2641, https://doi.org/10.1002/adfm.201102839.
[27] K. Wang, X. Dong, C. Zhao, X. Qian, Y. Xu, Facile synthesis of Cu_2O/CuO/RGO nanocomposite and its superior cyclability in supercapacitor, Electrochem. Acta 152 (2015) 433–442, https://doi.org/10.1016/j.electacta.2014.11.171.
[28] H. Zhang, P. Xu, G. Du, Z. Chen, K. Oh, D. Pan, Z. Jiao, A facile one-step synthesis of TiO_2/graphene composites for photodegradation of methyl orange, Nano Res. 4 (2011) 274–283, https://doi.org/10.1007/s12274-010-0079-4.
[29] Y. Gao, D. Ma, C. Wang, J. Guan, X. Bao, Reduced graphene oxide as a catalyst for hydrogenation of nitrobenzene at room temperature, Chem. Commun. 47 (2011) 2432–2434, https://doi.org/10.1039/c0cc04420b.
[30] C. Bayindirli, M. Celik, R. Zan, Optimizing the thermophysical properties and combustion performance of biodiesel by graphite and reduced graphene oxide nanoparticle fuel additive, Eng. Sci. Technol. Int. J. 158 (2018) 41–58, https://doi.org/10.1016/j.jestch.2022.101295.
[31] N.S. Hosseini, J. Hasanzadeh, A.A. Ziabari, A comparative study on the structure, morphology and ethanol sensitivity of ZnO thin films alloyed with graphene oxide and reduced graphene oxide, Opt. Quant. Electron. 54 (2022) 662, https://doi.org/10.1007/s11082-022-04029-4.
[32] N.S. Hosseini, J. Hasanzadeh, A.A. Ziabari, Synthesis, characterization and comparative gas sensing study of ZnO–GO and ZnO–rGO compounds, Acta Phys. Pol., A 141 (2022) 591–596, https://doi.org/10.12693/APhysPolA.141.591.
[33] A. Jiříčková, O. Jankovský, Z. Sofer, D. Sedmidubský, Synthesis and applications of graphene oxide, Materials 15 (2022) 920, https://doi.org/10.3390/ma15030920.
[34] Y. Shen, S. Yang, P. Zhou, Q. Sun, P. Wang, L. Wan, J. Li, L. Chen, X. Wang, S. Ding, D.W. Zhang, Evolution of the band-gap and optical properties of graphene oxide with controllable reduction level, Carbon 62 (2013) 157–164, https://doi.org/10.1016/j.carbon.2013.06.007.
[35] D.A. Sokolov, Y.V. Morozov, M.P. McDonald, F. Vietmeyer, J.H. Hodak, M. Kuno, Direct observation of single layer graphene oxide reduction through spatially resolved, single sheet absorption/emission microscopy, Nano Lett. 14 (2014) 3172–3179, https://doi.org/10.1021/nl500485n.
[36] N. Murugesan, S. Suresh, M. Kandasamy, S. Murugesan, N. Pugazhenthiran, S. K. Kumar, Enhancing selectivity of solar absorber using reduced graphene oxide modified nickel oxide nanocomposite thin films, Sol. Energy 247 (2022) 185–195, https://doi.org/10.1016/j.solener.2022.10.016.
[37] T.K. Das, P. Bhawal, S. Ganguly, S. Mondal, N.C. Das, A facile green synthesis of amino acid boosted Ag decorated reduced graphene oxide nanocomposites and its catalytic activity towards 4-nitrophenol reduction, Surface. Interfac. 13 (2018) 79–91, https://doi.org/10.1016/j.surfin.2018.08.004.
[38] P. Lin, Q. Yan, Y. Chen, X. Li, Z. Cheng, Dispersion and assembly of reduced graphene oxide in chiral nematic liquid crystals by charged two-dimensional nanosurfactants, Chem. Eng. J. 334 (2018) 1023–1033, https://doi.org/10.1016/j.cej.2017.09.195.
[39] M.M. Rahman, Z.-T. Jiang, C.-Y. Yin, L.S. Chuah, H.-L. Lee, A. Amri, B.-M. Goh, B. J. Wood, C. Creagh, N. Mondinos, M. Altarawneh, B.Z. Dlugogorski, Structural thermal stability of graphene oxide-doped copper–cobalt oxide coatings as a solar selective surface, J. Mater. Sci. Technol. 32 (2016) 1179–1191, https://doi.org/10.1016/j.jmst.2016.09.002.
[40] N.M. Huang, H.N. Lim, C.H. Chia, M.A. Yarmo, M.R. Muhamad, Simple room-temperature preparation of high-yield large-area graphene oxide, Int. J. Nanomed. 6 (2011) 3443–3448, https://doi.org/10.2147/ijn.s26812.
[41] G. Katumba, G. Makiwa, T.R. Baisitse, L. Olumekor, A. Forbes, E. Wackelgard, Solar selective absorber functionality of carbon nanoparticles embedded in SiO_2, ZnO and NiO matrices, Phys. Status Solidi C 5 (2008) 549–551, https://doi.org/10.1002/pssc.200776823.
[42] S. Thambidurai, P. Gowthaman, M. Venkatachalam, S. Suresh, M. Kandasamy, Morphology dependent photovoltaic performance of zinc oxide-cobalt oxide nanoparticle/nanorod composites synthesized by simple chemical co-precipitation method, J. Alloys Compd. 852 (2021), 156997, https://doi.org/10.1016/j.jallcom.2020.156997.
[43] A. Rousta, D. Dorranian, M. Elahi, Electrophoretic deposition of cobalt oxide nanoparticles on aluminium substrate, Surf. Eng. 36 (2020) 919–928, https://doi.org/10.1080/02670844.2019.1689899.
[44] N. Lenin, R.R. Kanna, K. Sakthipandi, A.S. Kumar, Structural, electrical and magnetic properties of $NiLa_xFe_{2-x}O_4$ nanoferrites, Mater. Chem. Phys. 212 (2018) 385–393, https://doi.org/10.1016/j.matchemphys.2018.03.062.
[45] A.A. Ziabari, A.B. Khatibani, Optical properties and thermal stability of solar selective absorbers based on Co–Al_2O_3 cermets, Chin. J. Phys. 55 (2017) 876–885, https://doi.org/10.1016/j.cjph.2017.02.015.
[46] X.-H. Gao, X.-L. Qiu, X.-T. Li, W. Theiss, B.-H. Chen, H.-X. Guo, T.-H. Zhou, G. Liu, Structure, thermal stability and optical simulation of ZrB_2 based spectrally selective solar absorber coatings, Sol. Energy Mater. Sol. Cells 193 (2019) 178–183, https://doi.org/10.1016/j.solmat.2018.12.040.
[47] H.C. Barshilia, N. Selvakumar, K.S. Rajam, A. Biswas, Optical properties and thermal stability of TiAlN/AlON tandem absorber prepared by reactive DC/RF magnetron sputtering, Sol. Energy Mater. Sol. Cells 92 (2008) 1425–1433, https://doi.org/10.1016/j.solmat.2008.06.004.
[48] X.-L. Qiu, X.-H. Gao, C.-Y. He, B.-H. Chen, G. Liu, Structure, optical simulation and thermal stability of the HfB_2-based high-temperature solar selective absorbing coatings, RSC Adv. 9 (2019) 29726–29733, https://doi.org/10.1039/c9ra05014k.
[49] B. Li, D. Qi, X. Wang, F. Wang, Y. Nie, R. Gong, Enhanced spectra selectivity of solar absorber film with Ti/Si_3N_4 photonic structures, Mater. Lett. 201 (2017) 5–8, https://doi.org/10.1016/j.matlet.2017.04.109.
[50] M. He, Y. Wang, H. Wang, R. Chen, A one-step sol–gel route derived Ag–CuO film as a novel solar selective absorber, Sol. Energy Mater. Sol. Cells 144 (2016) 264–272, https://doi.org/10.1016/j.solmat.2015.09.025.
[51] Z. Wu, F. Chen, Z. Xuan, Y. Chen, W. Shi, X. Liu, S. Wang, High energy efficient and thermally stable solar selective absorber constructed with TiN_xO_y based multilayers, Opt. Mater. Express 10 (2020) 733–741, https://doi.org/10.1364/ome.384483.
[52] I. Lorite, J.J. Romero, J.F. Fernandez, Effects of the agglomeration state on the Raman properties of Co_3O_4 nanoparticles, J. Raman Spectrosc. 43 (2012) 1443–1448, https://doi.org/10.1002/jrs.4098.
[53] M. Rashad, M. Rusing, G. Berth, K. Lischka, A. Pawlis, CuO and Co_3O_4 nanoparticles: synthesis, characterizations, and Raman spectroscopy, J. Nanomater. 2013 (2013), 714853, https://doi.org/10.1155/2013/714853.